Biosensors and Bioelectronics 130 (2019) 55–64

Contents lists available at ScienceDirect

Biosensors and Bioelectronics

journal homepage: www.elsevier.com/locate/bios

Sensitivity enhancement of cloth-based closed bipolar electrochemiluminescence glucose sensor via electrode decoration with chitosan/multi-walled carbon nanotubes/graphene quantum dots-gold nanoparticles

Dan Wang[1], Yi Liang[1], Yan Su[1], Qiuping Shang, Chunsun Zhang*

MOE Key Laboratory of Laser Life Science & Institute of Laser Life Science, College of Biophotonics, South China Normal University, Guangzhou 510631, China

ARTICLE INFO

Keywords:
Microfluidic cloth-based analytical devices
Closed bipolar electrode
Electrochemiluminescence
Multi-walled carbon nanotubes
Graphene quantum dots-gold nanoparticles
Glucose detection

ABSTRACT

In this work, a novel facile closed bipolar electrochemiluminescence (C-BP-ECL) sensor has been developed for highly sensitive detection of glucose based on the integration of chitosan (CS), poly(diallyldimethylammonium chloride)-functioned multi-walled carbon nanotubes (PDDA-MWCNTs) and graphene quantum dots-gold nanoparticles (GQDs-AuNPs) on the wax/carbon ink-screen-printed cloth-based device. When CS, PDDA-MWCNTs and GQDs-AuNPs are successively decorated onto the cathode of closed bipolar electrode (C-BPE), the C-BPE anode can emit much stronger C-BP-ECL signals. Moreover, the cathodic decoration of the C-BPE can generate a stronger ECL signal in comparison with its anodic decoration. Under optimized conditions, glucose can be detected in the range of 0.1–5000 μM, and the limit of detection is estimated to be 64 nM, which is about three orders of magnitude lower than that in case of the bare C-BPE cathode (31 μM). It has been shown that the proposed sensor has high detection sensitivity, wide dynamic range, and as well acceptable reproducibility, selectivity and stability. Finally, the applicability and validity of the C-BP-ECL sensor are demonstrated for the detection of glucose in human serum samples. We believe that this novel highly-sensitive sensor will have potential applications in various areas such as clinical diagnosis, food analysis and environmental monitoring.

1. Introduction

Glucose is a major component of animal and plant carbohydrates, and is one of the essential substances for life activities. Thus, its efficient and highly sensitive detection is important in many fields. Specially, the level of glucose in blood is a significant parameter in clinical medicine, as a high blood glucose concentration can cause diabetes mellitus that is a major risk factor in many diseases such as kidney failure, heart disease or blindness (Wang, 2008). Additionally, besides the need for glucose monitoring in the case of diabetes patients, it is also essential for nondiabetic acute care patients to control glucose levels (Matz et al., 2006).

Since the initial concept of glucose enzyme electrodes was proposed (Clark and Lyons, 1962), the development of glucose sensors has been a focal subject. Therefore, a huge amount of glucose sensors have been reported, and the detection methods include surface-enhanced Raman scattering (Hu et al., 2017), fluorometry (Liu et al., 2018a), colorimetry (Karim et al., 2018), chemiluminescence (Li et al., 2017), electrochemistry (Yao and Zhang, 2016), electrochemiluminescence (ECL) (Jiang et al., 2017) and so on. Among these methods, ECL is a very attractive technique, since it combines the simplicity of electrochemistry with inherent sensitivity and wide dynamic range of the chemiluminescence method. Importantly, ECL sensors usually have lots of advantages, including strong versatility, high sensitivity, low background, great selectivity, ease of control, and simplified optical set-up.

In 2001, ECL was first introduced to the bipolar electrode (BPE) system as a signal reporting method (Arora et al., 2001). Since then, the bipolar ECL (BP-ECL) has attracted considerable attention, and been widely applied to various sensing devices (Bouffier et al., 2016). BP-ECL combines the advantages of ECL and BPE systems. Especially, it exploits the wireless nature of BPEs for fascinating applications that are either impossible or inconvenient to achieve using conventional wired electrodes. A BPE is an electrically conductive material that is immersed into a solution (open BPE, O-BPE) or two separated solutions (closed

* Corresponding author.
E-mail addresses: zhangcs@scnu.edu.cn, zhangcs_scnu@126.com (C. Zhang).
[1] These authors contributed equally to this work.

https://doi.org/10.1016/j.bios.2019.01.027
Received 9 September 2018; Received in revised form 11 December 2018; Accepted 10 January 2019
Available online 21 January 2019
0956-5663/

BPE, C-BPE). The BP-ECL using a C-BPE (C-BP-ECL) is a good choice, because the anode and cathode of the BPE are separated into two physically isolated compartments (Zhang and Ding, 2017; Ge et al., 2018). Besides, C-BP-ECL possesses high current efficiency (100% in theory) (Zhang et al., 2017). Since its introduction in 2012 (Chang et al., 2012), however, C-BP-ECL is often performed in microfluidic devices, and relatively expensive and complicated microfluidic technologies are often required. Moreover, bulky and costly off-chip infrastructures are usually needed. These limitations may prevent its wide applications.

During the past years, microfluidic paper- or cloth-based analytical devices (μPADs or μCADs) have become powerful tools that have the potential to meet the 'ASSURED' characteristics—affordable, sensitive, specific, user-friendly, rapid and robust, equipment-free, and delivered to end-users. Generally, μPADs or μCADs combine the advantages of disposability, biocompatibility, flexibility, portability and being economic, with complex function (such as integrated elements for fluid flow controls (Fu and Downs, 2017) and dual-mode detection (Sun et al., 2018; Wang et al., 2018)) and multiplexed analysis of conventional lab-on-chip analytical devices (Yamada et al., 2017; Nilghaz et al., 2013). Recently, several simple and low-cost C-BP-ECL μPADs (Feng et al., 2014, 2015; Zhang et al., 2016b; Lu et al., 2016; Liu et al., 2018b) have been introduced. However, these μPADs still have some limitations as follows: the choice of paper in μPADs seems to be too narrow; the paper substrate still has a relatively high cost; μPADs have low tensile strength, flexibility and durability, and bad "wet strength"; and paper has usually relatively less interstitial spaces for flow channels (Liu et al., 2017). Fortunately, μCADs can circumvent the above-mentioned limitations. Recently, our group has developed a cloth-based microfluidic device for C-BP-ECL application (Liu et al., 2016). The proposed C-BP-ECL μCADs have two attracting features: strong flexibility and extremely low cost. In addition, they are manufactured with inexpensive and easily obtained materials, and only require a simple fabrication and assembly process. However, our previous C-BP-ECL μCADs have a poor sensitivity for glucose detection, with a detection limit of up to 0.195 mM (Liu et al., 2016).

As we know, nanoscale science and engineering hold great promise for the fabrication of novel sensors that offer stronger signal response and higher detection sensitivity. Generally, nanostructured materials used for sensor fabrication show better physical, electrical and catalytic properties in comparison with their bulk counterparts. Over the last decade, some nanomaterials have been used in conventional three-electrode luminol-H_2O_2 ECL sensors for glucose detection, including multi-walled carbon nanotubes (MWCNTs) (Lin et al., 2008; Qiu et al., 2009; Zhou et al., 2014), gold nanoparticles (AuNPs) (Liu et al., 2008; Zhong et al., 2014), MWCNTs-AuNPs (Haghighi et al., 2011), graphitic-phase carbon nitride-supported Au nanocomposites (Au-g-C_3N_4) (Jiang et al., 2017), AuNPs assembled polyaniline nanowires (Lou et al., 2017), MWCNTs-palladium NPs (Chen et al., 2009), fullerene (C_{60}) (Ye et al., 2014), graphene quantum dots–luminol–Ag nanoparticles (GQDs-luminol-AgNPs) nanocomposites (Salehnia et al., 2018), platinum nanoflowers/graphene oxide (PtNFs/GO) (Tian et al., 2014), and poly (luminol–aniline) nanowires composite (PLANC) (Li et al., 2010). Generally, the nanomaterials in these ECL sensors provide a high effective surface area and enhance the mass transfer; moreover they can efficiently interact with some species and promote the transmission of electrons. Therefore, the relatively sensitive glucose measurement can be obtained. However, nanomaterials have rarely been applied onto the on-chip enzymatic electrode-based BP-ECL glucose sensors (Xiao et al., 2017). To our knowledge, to date no work has yet focused on the use of certain nanomaterial(s) for enhancing the C-BP-ECL performance for glucose determination.

In this work, we have taken advantages of poly(diallyldimethylammonium chloride)-functioned MWCNTs (PDDA-MWCNTs) and graphene quantum dots-gold nanoparticles (GQDs-AuNPs) to construct a highly sensitive cloth-based C-BP-ECL glucose sensor. GQD consists of a single to several layers of graphene sheets several nanometers in lateral size (Budyka, 2019), and thus GQDs have the graphene structure with one layer or multilayers of sp^2 hybridized carbon atoms packed into a unique planar structure. Compared with other quantum dots (QDs), GQDs have some attractive advantages such as low cost, low toxicity, large special surface area, robust chemical inertness, unique electro-optical properties, good biocompatibility and water-solubility, and environmental friendliness. However, sometimes it will be difficult to apply GQDs directly in bio-sensing. For example, the good solubility makes GQDs difficult to be immobilized on the surfaces of electrodes (Dong et al., 2015). In addition, a complex bio-labeling may be required for GQDs. To address these issues, the coupled use of GQDs with other metal nanomaterials (Salehnia et al., 2018; Dong et al., 2015) can be performed to provide the integrated properties of two components. Among metal nanomaterials, AuNPs are very attractive because of their low electron transfer resistance, excellent electro-catalytic activity, good biocompatibility and versatile surface modification (Lou et al., 2017). In this work, to develop a relatively simple and sensitive diagnostic method, GQDs are used to reduce $HAuCl_4$ to prepare the GQDs-AuNPs nanocomposites. Furthermore, PDDA-MWCNTs are used to well immobilize the GQDs-AuNPs on the carbon electrode. PDDA can be applied not only to improve the dispersion of MWCNTs in aqueous solutions, but also to well adsorb oppositely charged nanoparticles (Zhang et al., 2016a). Also, the presence of MWCNTs with excellent electrical conductivity and large surface-to-volume ratio maybe increases the active area of the electrode surface and facilitates the electron and mass transfer, and therefore the ECL intensity can be enhanced greatly (Lin et al., 2008; Qiu et al., 2009; Haghighi et al., 2011; Zhou et al., 2014; Xiao et al., 2017).

In the presented C-BP-ECL sensor, the cathode and anode of the carbon ink-screen-printed C-BPE are connected onto the wax-screen-printed supporting channel and reporting channel, respectively. The proposed glucose sensing platform can provide several attractive features as follows. Firstly, the cloth-based devices are uncomplicated in fabrication, low in cost, and do not need any specialized persons. Secondly, the chitosan (CS), PDDA-MWCNTs and GQDs-AuNPs are decorated onto the C-BPE cathode (CBC), while the C-BPE anode (CBA) is modified by glucose oxidase (GOD) for luminol-based ECL measurement of glucose. Such a sensing protocol can provide a relatively strong C-BP-ECL signal. Thirdly, the optimized sensor shows excellent sensitivity, acceptable reproducibility and stability, wide dynamic range and high selectivity for the detection of glucose. Especially, the detection limit of glucose with electrode decoration with PDDA-MWCNTs and GQDs-AuNPs (64 nM) is about three orders of magnitude lower than that in case of the bare CBC (31 μM). Finally, the glucose levels in complex human serum samples are measured on the proposed sensor, with acceptable similarity to those obtained by the clinical colorimetry and the commercial glucometer.

2. Experimental section

2.1. Chemicals, materials and instrumentation

The details for chemicals, materials and apparatuses used in this work are available in the Supplementary information (SI).

2.2. Pretreatment of MWCNTs

The pretreatment of MWCNTs was performed according to the reported methods with a slight modification (Chen et al., 2009; Zhang et al., 2016a). Firstly, in a typical acid-treatment procedure, 1 g of MWCNTs were submerged in a 40 mL mixture of H_2SO_4 (95–98%) and HNO_3 (65–68%) (v/v, 3:1), and then put into an ultrasonic cleaner, keeping a continuous 8 h ultrasonic concussion at room temperature. Afterwards, a black solid was obtained by centrifugally filtrating and water washing several times (until the pH of the washed solution

became to be ~ 7.0). The black solid was dried for 24 h in a 80 °C oven. Next, 0.1 g acid-treated MWCNTs were dispersed into 20 mL of 0.25 wt % PDDA aqueous solution containing 0.5 M NaCl, followed by being ultrasonicated for 1 h to obtain a homogeneous black suspension. Then, the resulting dispersion was centrifuged and washed with water three times to remove the redundant PDDA. Finally, the product of PDDA-MWCNTs was dispersed in water to obtain 5 g L^{-1} of PDDA-MWCNTs. The resulting solution was stored at 4 °C before use, and was sonicated for about 2 min when in use.

2.3. Preparation of GQDs-AuNPs

GQDs-AuNPs hybrid nanomaterials were prepared by a simple reduction method. In brief, gold colloids were prepared by the reduction of $HAuCl_4$ with GQDs. In a typical preparation procedure, 0.5 mL of $HAuCl_4$ solution (0.5%, w/w) was rapidly added into 25 mL of boiling GQDs solution (0.02 g L^{-1}) under magnetic stirring. The solution boiled at 100 °C for 30 min until it turned crimson. Subsequently, the solution was naturally cooled to room temperature when the heating source was removed and the stirring was continued. The solution of hybrid nanomaterials was centrifuged and washed with water in turn for three times to obtain the desired GQDs-AuNPs. Finally, these nanocomposites were dispersed into 25 mL water for further use.

2.4. Preparation of cloth-based C-BP-ECL sensor

The preparation processes of the proposed sensor include the fabrication of cloth-based devices, decoration of nanomaterials on the CBC and modification of GOD on the CBA. For fabricating the cloth-based devices, the electrode-screen and channel-screen were custom-made with six similar units. Each patterned unit on the electrode-screen consisted of one C-BPE (3 mm × 13 mm) and two driving electrodes (5 mm × 8 mm), while each unit on the channel-screen included a pair of supporting and reporting channels (6 mm × 13 mm). Using these two screens, the cloth-based devices could be fabricated quickly (Fig. 1**A**). In short, the electrode-screen was fixed over an appropriately-sized cloth (6 cm × 10 cm), and was then screen-printed by carbon ink, followed by baking the ink-patterned cloth for 15 min in a 90 °C oven (Steps 1–3). After that, the channel-screen was placed on the back of the electrode-patterned cloth, and rubbed in turn with a green crayon (i.e. solid wax) and a smooth utensil (Steps 4–5). Subsequently, the channel-screen and cloth was baked for ~ 3 s on a 120 °C heating board to melt the wax into the cloth (Step 6). Finally, the cloth and channel-screen were removed from the heating board, and separated from each other to form the cloth-based devices (Step 7).

As shown in lower panels of Fig. 1**B**, the C-PBE poles of each cloth-based device could be modified to construct the glucose sensor. Firstly, 1.5 μL of 1.0% (v/v) CS solution was dropped onto the surface of the CBC, and dried for a few minutes at room temperature, followed by applying a repeated step for another 1.5 μL CS solution to prepare the CS-modified CBC (labeled as CS/CBC). In a way similar to that 3 μL CS solution (1.5 μL each time) was added and dried, 3 μL of 5 g L^{-1} PDDA-MWCNTs solution was applied onto the surface of CS/CBC to create the PDDA-MWCNTs/CS-modified CBC (labeled as PDDA-MWCNTs/CS/CBC). Subsequently, in a similar way, 3 μL solution of GQDs-AuNPs was spotted onto the PDDA-MWCNTs/CS/CBC to make the desired CBC (labeled as GQDs-AuNPs/PDDA-MWCNTs/CS/CBC). Notably, the abovementioned three solutions were dropped twice onto the CBC to obtain a more uniform and stable distribution. Next, the CBA was further modified with GOD for glucose measurement, where 1.5 μL of GOD solution was dropped onto the surface of the CBA, followed by being dried for ~ 2 min at room temperature, and 1 μL of similar enzyme solution was then added onto the anode. Here, the optimized enzymatic modification process could produce a stronger ECL signal (Fig. S1), possibly because it prevented the enzyme solution from flowing out of the electrode surface and caused more efficient immobilization of enzyme molecules to the electrode surface. Finally, the as-prepared sensor was stored in a 4 °C refrigerator when it was not used.

2.5. C-BP-ECL assay procedure and data analysis

The C-BP-ECL assay procedure was described as follows. Firstly, the cloth-based device was placed on a self-made support and fixed by the clips, and then 15 μL luminol/glucose-containing assay solution and carbonate buffer solution (CBS) (containing 200 mM Na_2CO_3 and 130 mM $NaHCO_3$, pH 10.75) were added into the reporting and supporting channels, respectively. Secondly, the support was placed into the black box of the lab-assembled ECL measurement and analysis system, where the image of the device could appear clearly on the PC screen by adjusting the movable mechanical stage and the focus-adjustable bracket. Meanwhile, an adequate waiting time was needed for the solutions to fill the channels and for enzymatically-catalyzed production of H_2O_2. Finally, the CCD automatic imaging function was started, and an appropriate driving voltage (E_{tot}) was applied to trigger the C-BP-ECL. As we know, it is the interfacial potential difference ($\Delta\varphi$) that drives the faradic reactions associated with the C-BP-ECL (Wang et al., 2017). As seen from the potential profile in the upper panel of Fig. 1**B**, the applied potential equals the sum of the four interfacial potential differences ($\Delta\varphi_a'$, $\Delta\varphi_c$, $\Delta\varphi_a$, and $\Delta\varphi_c'$) and potential dropped on the solutions and C-BPE. At the CBA in the reporting channel, the anodic interfacial potential difference ($\Delta\varphi_a$) drives the ECL reactions. If the applied potential across two cloth channels is sufficiently high, faradic reactions occur at both poles of the C-BPE, one for oxidation at the CBA and the other for simultaneous reduction at the CBC. Fig. 1**C** schematically shows the proposed assay principle for glucose detection. Here, it should be noted that unless otherwise stated, all the assays were performed at a room temperature of less than 30 °C.

The C-BP-ECL images were taken by the CCD, and were recorded in the JPEG format. They were batch-cut to a size of 700 × 500 pixels by the software nEO iMAGING 4.4.1 (Shenzhen Thunder Net Culture Co., Ltd., Shenzhen, China), and then the batch pictures were analyzed by an automated image-processing program which was developed in Matlab R2015a (MathWorks company, USA). As a result, the average gray value of each picture was obtained, and the image with the maximum ECL intensity (i.e. the maximum photon counts) was easily found. In this work, the luminous intensity of such an image was used as the analytical signal to quantify each assay. For further analysis, the acquired ECL data were imported into Origin 7.0 (OriginLab Corporation, MA, USA).

3. Results and discussion

3.1. Characterization of PDDA-MWCNTs and GQDs-AuNPs

In the presented work, MWCNTs were initially treated by acidification and ultrasonic agitation, and thus they were not only chemically shortened but also functioned with carboxyl groups on their tips and any defect in the side walls. As a result, PDDA, a cationic polyeletrolyte, could be adsorbed on the surface of the MWCNTs by electrostatic interaction between carboxyl groups on the MWCNTs and polyeletrolyte chains (Cui et al., 2008). As indicated in the TEM image of Fig. 2**A**, long and typical tube-like MWCNTs could be well-dispersed in aqueous solution, which may be attributed to the fact that PDDA plays the poles of dispersing agent, inhibiting the strong π–π stacking interaction between MWCNTs (Amatatongchai et al., 2015). Note that the unpretreated MWCNTs (5 g L^{-1}) aggregated soon and deposited in water after standing for several minute, while the pretreated MWCNTs with a similar concentration could remain well dispersed in water for at least 6 months. The TEM technology was also used to investigate the morphology, structure and dispersion of the GQDs-AuNPs. As we know, the reductive groups on GQDs (like hydroxyl groups) can reduce $HAuCl_4$ into AuNPs. Fig. 2**B** shows the TEM image of the obtained

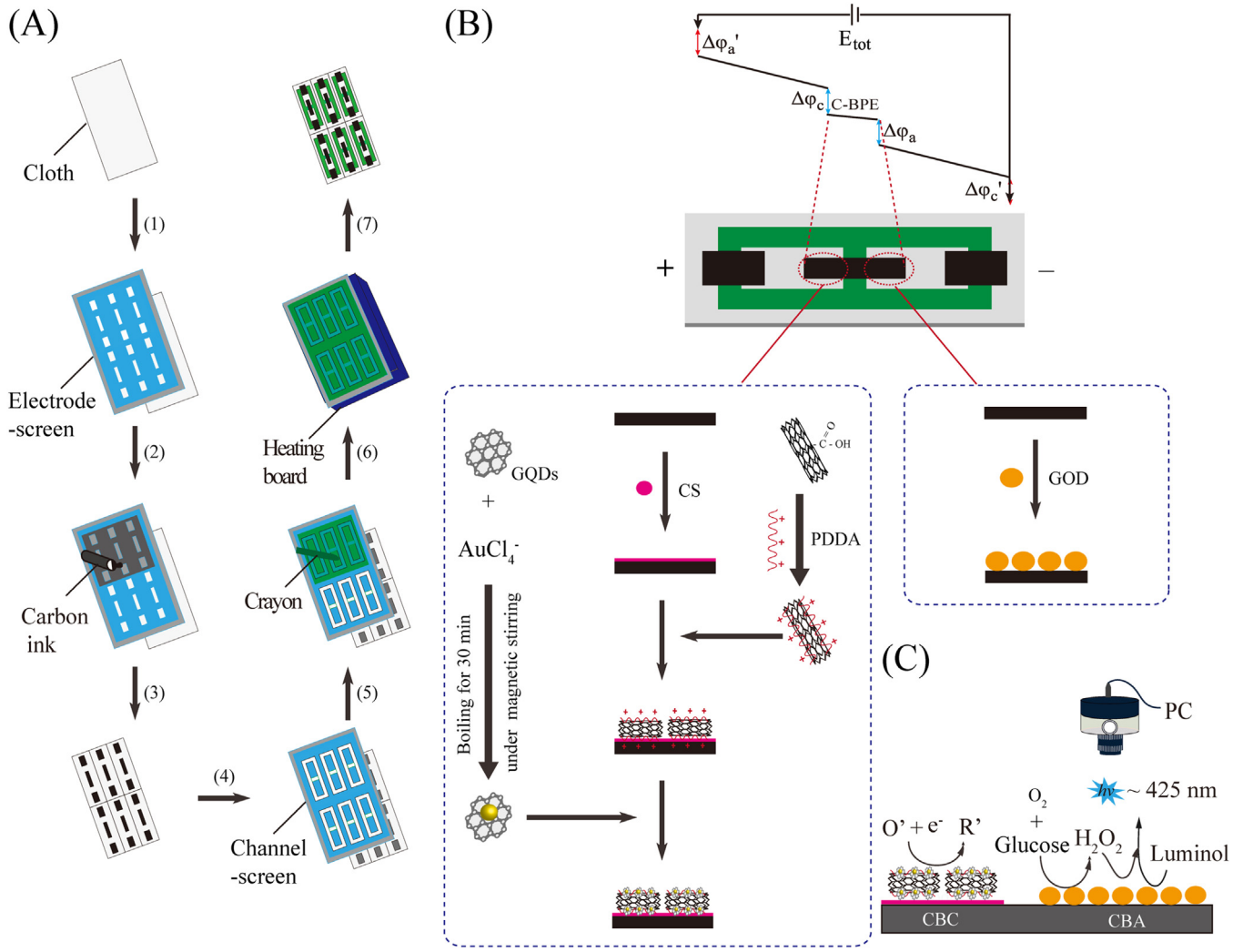

Fig. 1. Schematic illustration for the preparation and sensing principle of cloth-based C-BP-ECL glucose sensor. (**A**) Screen-printing procedure for fabrication of cloth-based devices. The electrode-screen is placed on the cloth (1); carbon ink is screen-printed onto the cloth (2); the carbon ink-patterned cloth is separated from the screen and dried at an appropriate temperature (3); the channel-screen is fixed on the back of the electrode-patterned cloth (4); the screen is successively rubbed with a crayon and a smooth utensil (5); the screen and cloth is placed on the heating board together (6); and the screen and cloth are taken away from the heating board, and separated from each other to form the desired cloth-based devices (7). (**B**) Potential profile across two cloth channels and corresponding decoration of GQDs-AuNPs/PDDA-MWCNTs/CS and GOD on the C-BPE cathode and anode (CBC and CBA). Here, $\Delta\varphi_a$ and $\Delta\varphi_c$ represent the interfacial potential differences at the CBA/solution and CBC/solution, respectively. $\Delta\varphi_a'$ and $\Delta\varphi_c'$ represent the interfacial potential differences at the anode/solution and cathode/solution of the driving electrodes, respectively. (**C**) Luminol-based C-BP-ECL sensing principle for glucose detection.

GQDs-AuNPs nano-hybrids. It can be seen that GQDs-AuNPs were about 15 nm in size without regular morphologies. The UV–vis absorption spectroscopy was used to further characterize the component of the nanomaterials. The samples of both GQDs and GQDs-AuNPs showed a shoulder peak at about 360 nm, which corresponded to the n-π * transitions of C-O bonds (Fig. 2**C**). The GQDs-AuNPs showed a characteristic absorption peak centered at around 520 nm, representing the presence of Au particles in nano-scale by the surface plasmon effect. Similar to the TEM images (Fig. 2**B**), these absorption peaks also demonstrate that the GQDs and AuNPs were well distributed in the GQDs-AuNPs nano-hybrids.

3.2. Microscopic, electrochemical and ECL characterization of the proposed sensor

Based on the two screen-printing processes and the modifications of nanomaterials and GOD on the corresponding C-BPE poles, the desired cloth-based sensor could be fabricated. Fig. 3 shows the picture, SEM images and electrochemical characteristics of a typical sensing device. As shown in Fig. 3**A**, the proposed fabrication method could provide an acceptable hydrophilic/hydrophobic contrast to define the cloth-based device. Also, after the electrodes were one-step fabricated onto the cloth, two wax barrier-enclosed channels could be processed onto the cloth to well contain these electrodes if the channel-screen was fixed on the back of the electrode-patterned cloth. It can been seen from Fig. S2A that the solution could be restricted in the cloth channel. On the contrary, when the wax screen-printing was applied onto the front of the patterned cloth, wax barriers could not be well formed in the electrode region, and the solution would flow out of the cloth channel (Fig. S2B). The possible reason for this phenomenon is that wax could not penetrate the carbon electrode into the cloth. Fig. 3**B-D** shows the SEM images of three different functional regions on the screen-printed cloth. For the unwaxed cloth channels, the structure of multiple gaps between the single fibers (~ 10 μm) was clearly observed, indicating that the bare cloth could offer a good hydrophilic microenvironment (Fig. 3**B**). It can be seen from Fig. 3**C** that on account of the porous structure of the cloth, the screen-printed wax could well penetrate into the cloth to create the hydrophobic barrier. For screen-printed carbon electrodes, a

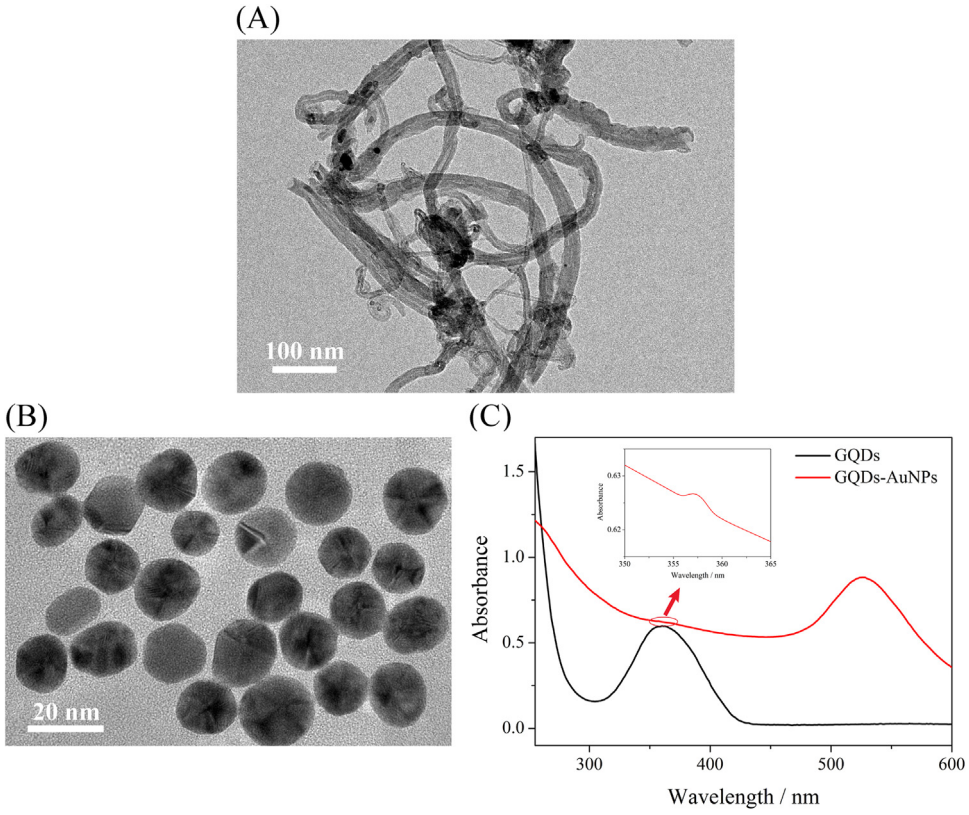

Fig. 2. Characterization of as-prepared nanomaterials. (**A**, **B**) TEM images of PDDA-MWCNTs and GQDs-AuNPs. (**C**) UV–vis absorption spectra of GQDs and GQDs-AuNPs.

continuous and dense carbon conducting layer could be found on the surface of the cloth, suggesting that an acceptable coverage of carbon materials on the surfaces of the cloth cellulose fibers was achieved (Fig. 3**D**). Fig. 3**E-G** displays typical SEM images of CS, PDDA-MWCNTs/CS, and GQDs-AuNPs/PDDA-MWCNTs/CS assembled on the CBC surfaces, respectively. It can be observed from these images that the corresponding film could be successfully formed on the CBC after the solutions of these substances were stepwise applied. Especially, the PDDA-MWCNTs could well absorb the GQDs-AuNPs to prepare the desired electrode decoration. It has been reported that PDDA easily forms standing thin films on the electrode surface, and interacts well with oppositely charged nanoparticles (Zhang et al., 2016a).

The electrochemical impedance spectroscopy (EIS) of the redox probe $Fe(CN)_6^{3-/4-}$ was employed to further monitor the features of the modified electrodes, because it is one of the most powerful and effective techniques to investigate the modification process. The semicircle diameter in the EIS equals to the electron transfer resistance (R_{et}), which controls the electron transfer kinetics of the redox probe at the electrode interface. When compared with the bare CBC (curve a in Fig. 3**H**), an obviously decreased R_{et} was obtained on the CS/CBC (curve b in Fig. 3**H**), possibly because the abundant amino groups adsorbed much more negatively charged $Fe(CN)_6^{3-/4-}$ to facilitate the interfacial electron transfer (Yan et al., 2012). When PDDA-MWCNTs and GQDs-AuNPs were successively modified onto the CS/CBC, continuous decrease in R_{et} was observed (curves c and d in Fig. 3**H**), which suggested that PDDA-MWCNTs and GQDs-AuNPs were excellent electronic conducting materials and could accelerate the electron transfer between $Fe(CN)_6^{3-/4-}$ probe and electrode. Besides, the cyclic voltammetry (CV) of $Fe(CN)_6^{3-/4-}$ was also used to affirm the assembly process of the electrodes. It can be observed that the current magnitude of the CS/CBC (curve b in Fig. 3**I**) is higher than that of the bare CBC (curve a in Fig. 3**I**), which can be ascribed to the foregoing electrostatic interaction between the probe $Fe(CN)_6^{3-/4-}$ and protonated amino groups of the CS film. When PDDA-MWCNTs and GQDs-AuNPs were applied in succession on the CS/CBC, a continuous increase in the peak current was found due to their good conductivity (curves c and d in Fig. 3**I**), which is consistent with the result of EIS.

To verify whether the proposed ECL sensor indeed worked as expected, C-BP-ECL was used to characterize the changes of the electrode behavior after each modification step, where the luminol (2 mM)/glucose (0, 50 or 250 μM)-containing assay solution (pH 10.5) and CBS (pH 10.75) were applied onto the reporting and supporting channels, respectively. As shown in Fig. 4, only weak signals at the C-BPE anodes were observed for the bare CBCs, but the signals were gradually enhanced as the CS, PDDA-MWCNTs and GQDs-AuNPs were applied step by step. In comparison with the ECL intensities using the bare CBC (about 0.60×10^6 counts at 50 μM and about 5.04×10^6 counts at 250 μM), the ECL intensities of GQDs-AuNPs/PDDA-MWCNTs/CS/CBC at 50 μM and 250 μM increased remarkably to be about 4.00×10^6 and 9.67×10^6 counts, respectively. Notably, under similar conditions, the enhancement effect of GQDs-AuNPs was higher than that of AuNPs, GQDs or simple mixture between AuNPs and GQDs (labeled as AuNPs + GQDs) in the absence (left four columns in Fig. S3) or presence (right four columns in Fig. S3) of PDDA-MWCNTs, which may be attributed to that certain hybrid nanostructures between GQDs and AuNPs were well formed and that the presence of AuNPs in these nano-hybrids gave rise to many more active sites with higher electrocatalytic activity. It also can be clearly seen from Fig. S3 that for each case the presence of PDDA-MWCNTs could enhance the ECL signal, indicating that PDDA-MWCNTs could facilitate reduction reactions in the supporting channel and improve the ECL intensity.

Furthermore, it has been observed that the enhancement effect of GQDs-AuNPs/PDDA-MWCNTs/CS/CBC was superior to that of the GQDs-AuNPs/PDDA-MWCNTs/CS assembled C-BPE anode (GQDs-AuNPs/PDDA-MWCNTs/CS/CBA) (Fig. S4). At present, we may have been unable to accurately pinpoint the source of this phenomenon, but

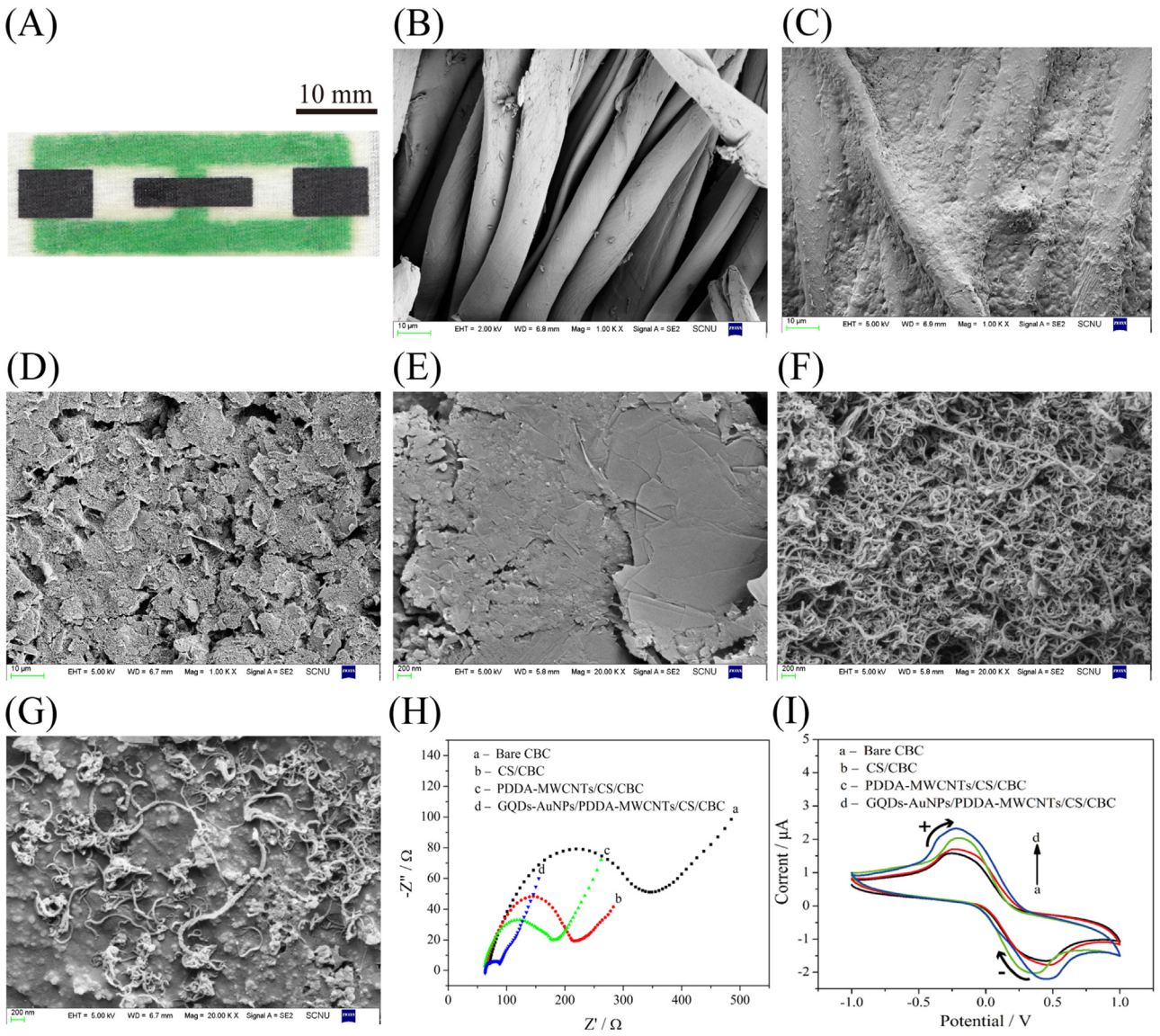

Fig. 3. Characterization of cloth-based devices. (**A**) Photo of a typical cloth-based C-BP-ECL sensor. (**B-G**) SEM images of the pure cloth (for the hydrophilic channels), wax-screen-printed cloth (for the hydrophobic barrier), bare CBC of carbon ink-screen-printed cloth, CS-modified CBC (CS/CBC), CS and PDDA-MWCNTs-modified CBC (PDDA-MWCNTs/CS/CBC), and as well CS, PDDA-MWCNTs and GQDs-AuNPs-modified CBC (GQDs-AuNPs/PDDA-MWCNTs/CS/CBC). (**H, I**) Impedance (Nyquist) plots and cyclic voltammograms of different electrodes. The electrochemical impedance spectroscopy (EIS) and cyclic voltammetry (CV) were performed in 10 mM $Fe(CN)_6^{3-/4-}$ solution (containing 0.5 M KCl) by a conventional three-electrode system including a bare or modified screen-printed carbon electrode as the working electrode, a Pt electrode as the auxiliary electrode and a Ag/AgCl electrode as the reference electrode. The CV was recorded in the potential range from −1.0 to 1.0 V at a scan rate of 100 mV s^{-1}, while the EIS was recorded in the frequency range of 0.1–100 kHz with an amplitude of 5 mV.

we suspect that one reason is that the nanomaterials modified on the CBC can promote some potential reduction reactions in the supporting channel, which enhances the rate of electron transfer between two poles of the C-BPE. It has been reported that MWCNTs can greatly catalyze the oxygen reduction reaction (ORR), and the ORR can proceed as $2H_2O + O_2 + 4e^- \rightarrow 4OH^-$ in alkaline solution (Zhang et al., 2014; Sang et al., 2016). In addition, GQDs contain many oxygenated functional groups such as carbonyl (-C=O), carboxyl (-COOH), epoxy (-O-) and hydroxyl (-OH) and thus reduced GQDs are easily produced ($GQDs + e^- \rightarrow GQDs^*$) (Gupta et al., 2017; Nie et al., 2018).

It is particularly noteworthy that the modification in the cathode may be of much importance. Besides that a relatively strong enhancement effect could be achieved, another reason is that the cathodic modification does not potentially interfere with the luminescence on the anode. After all, some nanomaterials will adversely affect the luminescence (Li et al., 2018). In addition, the cathodic modification may increase the possibility of other potential applications and integrated functions. For example, the modification in a single shared cathode maybe has the potential to be used for highly sensitive assays on multiple anodes.

It should be noted that the proposed ECL sensor had a very low cost for glucose measurement. Based on the used chemicals and materials, the cost of each sensing device was about $0.028 (Table S3). In this cost estimation, the equipment costs (ECL measurement and analysis system, DC power supply and computer) were not included. As seen from Table S3, the costs of CS, PDDA-MWCNTs and GQDs-AuNPs used in the electrode modification were extremely low. Note that the plastic support that was utilized to fix the sensor could be used repeatedly and therefore its cost was negligible.

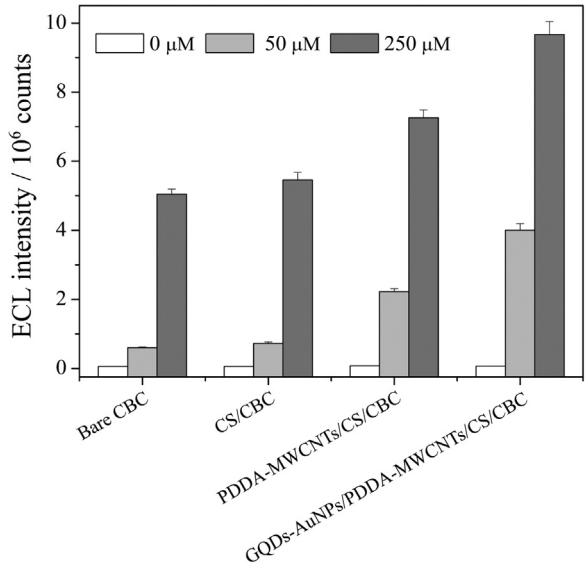

Fig. 4. C-BP-ECL intensities obtained using different cathode modifications. Experimental conditions: driving voltage (E_{tot})–8 V; concentration of glucose ([Glucose])–0, 50 and 250 μM; concentration of luminol ([Luminol])–1.5 mM; pH of reaction solution in the reporting channel/supporting channel (pH_{rc}/pH_{sc})–10.5/10.75; concentration of GOD ([GOD])–5 U μL^{-1}; and incubation time (t_i)–2 min. The error bars represent the standard deviations of five independent measurements from different devices.

3.3. Optimization of reaction conditions for the C-BP-ECL sensor

To better investigate the effect of the driving voltage (E_{tot}) in this sensor, C-BP-ECL measurements with ten different E_{tot} values were carried out. As shown in Fig. 5**A**, at a lower E_{tot} (e.g. 2.0 V), no ECL reaction was triggered at the C-BPEs. Upon increasing the value of E_{tot} gradually, the ECL intensity was increased. However, when the E_{tot} value exceeded 8.0 V, the ECL intensity decreased. The decrement of ECL signal may be due to the fast consumption of ECL reagents (Liu et al., 2018b). In addition, it has been reported that background reactions (e.g. oxidation of water) can be initiated under a high driving potential and they both chemically and physically interferes with ECL emission (Chang et al., 2012).

The effect of luminol concentration on the C-BP-ECL signal has been investigated in the range of 0.5–2.5 mM. As shown in Fig. 5**B**, the ECL intensity increased almost linearly with an increase in the concentration of luminol from 0.5 to 1.5 mM. However, the further increase of concentration could cause a rapid drop in ECL intensity, possibly because of the self-quenching effect (Zhu et al., 2002; Liu et al., 2018b). Therefore, 1.5 mM was chosen as the optimal concentration of luminol in this study. As is known, the luminol-based ECL reactions are more efficient in alkaline media, while higher pH value may inhibit enzyme activity because the optimal pH value for GOD activity is generally below the neutral pH. Therefore, to obtain better ECL sensing to glucose, the effect of pH of reaction solution in the reporting channel (pH_{rc}) was investigated in the range of 7.0–11.5. As seen from Fig. 5**C**, the sensor showed strongest ECL response to glucose at pH_{rc} 10.5, which was probably a compromise between the two optimal conditions. Similarly, the effect of pH of reaction solution in the supporting channel (pH_{sc}) was also studied. The result showed that the peak value of ECL intensity was obtained at pH_{sc} 10.75. As such, pH_{rc} and pH_{sc} were correspondingly optimized to be 10.5 and 10.75 for the later experiments.

The effects of GOD concentration and enzymatic reaction time (i.e. incubation time between glucose and GOD, t_i) on the C-BP-ECL response were also evaluated. As shown in Fig. 5**D**, a gradual increase in ECL intensity was observed when the enzymatic concentration was less than 5 U μL^{-1}. However, ECL intensity would not increase anymore at the concentrations above 5 U μL^{-1}. Thus, 5 U μL^{-1} was chosen as the optimum enzymatic concentration for the subsequent experiments. In the case of t_i, eight different lengths of t_i (between ~0 and 3.5 min) were investigated to evaluate this effect (Fig. 5**E**). For t_i of "~0 min", the assay was performed as quickly as possible after the reaction solutions were added onto the supporting and reporting channels, respectively. It has been observed that the intensity of ECL signal increased gradually with the increase of t_i, and then reached a plateau at more than 2 min, suggesting the maximum enzymatic oxidation of glucose to gluconic acid and H_2O_2. Considering the optimal analytical performance and development of the proposed method for rapid sample analysis, 2 min was selected as the best reaction time.

Temperature is always a key factor for ECL response and enzymatically-catalyzed reaction system. To evaluate this factor, the surface temperature of the cloth-based sensor (T_s) was precisely controlled to indirectly reflect the reaction temperature during ECL measurements. Simply, the cloth-based device was closely placed on the copper heating block, while the K-type thermocouple was mounted between the cloth-based device and the copper block to measure the T_s value (SI). As shown in Fig. 5**F**, the ECL intensity almost maintained constant with the increase of T_s from 10 to 30°C. However, when the value of T_s was higher than or equal to 35 °C, a distinct decrease in ECL intensity was observed. This phenomenon may be ascribed to the following factors. Firstly, the thermal movement of luminol radicals produced by oxidation of luminol was violent at higher temperatures, and so the increased chance of self-annihilation of luminol radicals caused the decreased ECL intensity (Zhao et al., 2011). Secondly, a higher temperature might have a negative effect on the enzyme activity. Thirdly, the evaporation of reaction solution could be accelerated at elevated temperatures, which might adversely influence the ECL reaction. At room temperature, however, such an evaporation loss during the C-BP-ECL was negligible.

3.4. Performance of the proposed sensor for glucose detection

Under optimized conditions, the cloth-based sensor with desirable cathodic modifications was firstly used for glucose detection. As shown in Fig. 6, ECL intensity gradually increased as the glucose concentration varied from 0.1 to 5000 μM, and as well ECL intensity increased linearly with the glucose concentration in the range of 0.1–20 μM (R^2 = 0.9986) (Insert in Fig. 6). The limit of detection (LOD) (defined as the concentration generating a signal three standard deviations higher than the blank) was estimated to be 64 nM. A comparative study was also performed using the sensor without any cathodic modifications. As shown in Fig. S5, the increased ECL signals were directly related to the glucose concentrations (50–10000 μM). A direct linear relationship between ECL intensity and glucose concentration from 50 to 175 μM (R^2 = 0.9925) was obtained (Insert in Fig. S5), and the LOD was 31 μM. Obviously, the detection limit in the case of cathodic modifications is about three orders of magnitude lower than that using the bare CBC. It is noted that compared with some other large-size or conventional on-chip ECL glucose sensors, the proposed sensor has the better detection sensitivity or range, and only needs simple and cheap fabrication techniques and facilities (Table S4). In addition, it can be seen from Table S4 that in comparison to other paper-, cloth- or thread-based ECL glucose measurements, the presented C-BP-ECL method could give a much lower detection limit.

3.5. Reproducibility, selectivity and stability of the proposed sensor

The reproducibility of the sensors was estimated by inter-assay and intra-assay relative standard deviations (RSDs) which were evaluated from the luminescent response of 0.1 mM glucose in C-BP-ECL sensors. The glucose assay using five different sensors independently fabricated on different batches (inter-assay) showed a RSD of 2.7%. For the assay

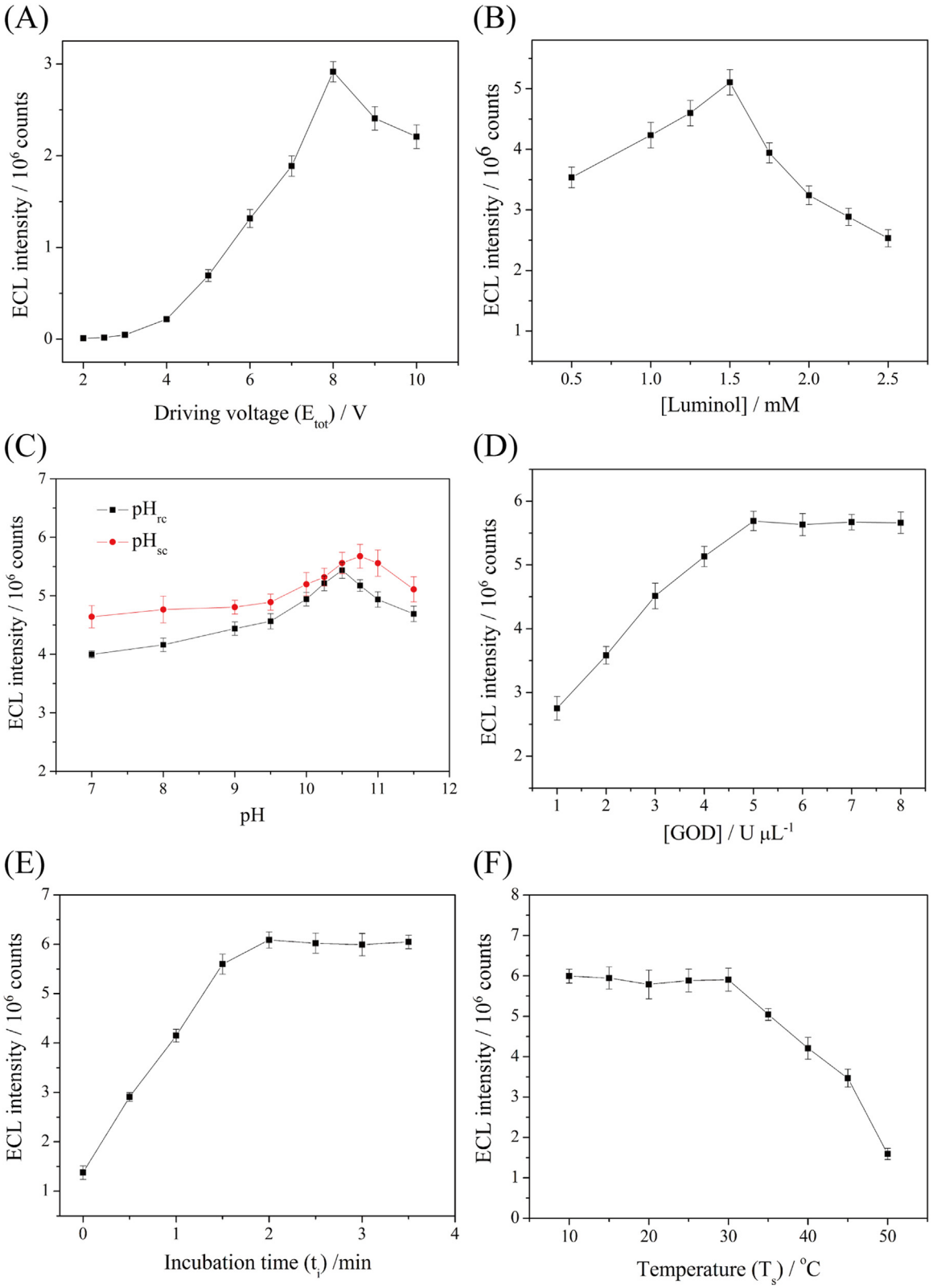

Fig. 5. Dependence of C-BP-ECL intensities on E_{tot} (**A**), [Luminol] (**B**), pH_{rc}/pH_{sc} (**C**), [GOD] (**D**), t_i (**E**), and surface temperature of the cloth-based device (T_s) (**F**). In panel (A), [Glucose]–100 μM, E_{tot}–2–10 V, [Luminol]–2 mM, pH_{rc}/pH_{sc}–10.5, [GOD]–5 U μL^{-1}, and t_i–1.5 min. In panel (B), [Glucose]–100 μM, E_{tot}–8 V, [Luminol]–0.5–2.5 mM, pH_{rc}/pH_{sc}–10.5, [GOD]–5 U μL^{-1}, and t_i–1.5 min. In panel (C), [Glucose]–100 μM, E_{tot}–8 V, [Luminol]–1.5 mM, pH_{rc}/pH_{sc}–7.0–11.5, [GOD]–5 U μL^{-1}, and t_i–1.5 min. In panel (D), [Glucose]–100 μM, E_{tot}–8 V, [Luminol]–1.5 mM, pH_{rc}/pH_{sc}–10.5/10.75, [GOD]–1–8 U μL^{-1}, and t_i–1.5 min. In panel (E), [Glucose]–100 μM, E_{tot}–8 V, [Luminol]–1.5 mM, pH_{rc}/pH_{sc}–10.5/10.75, [GOD]–5 U μL^{-1}, and t_i–0–3.5 min. In panel (F), [Glucose]–100 μM, E_{tot}–8 V, [Luminol]–1.5 mM, pH_{rc}/pH_{sc}–10.5/10.75, [GOD]–5 U μL^{-1}, t_i–2 min, and T_s–10–50 °C. The error bars represent the standard deviations of five independent measurements from different devices.

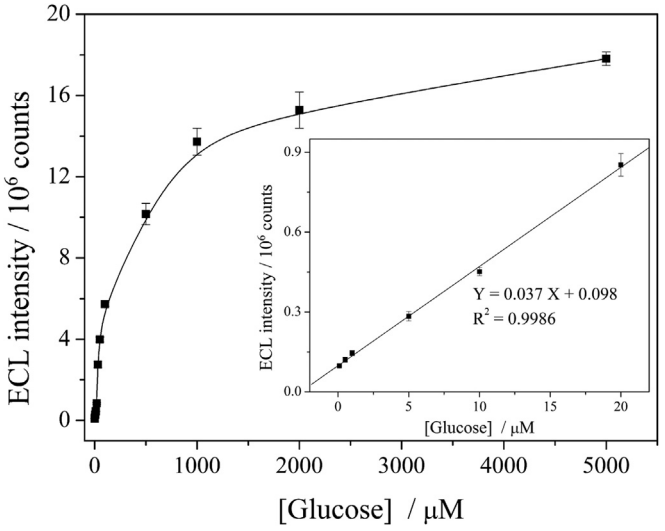

Fig. 6. Calibration curve for determination of glucose based on the proposed sensor. The insert showed that the ECL intensities could be linearly proportional to glucose concentrations in the ranges of 0.1–20 μM. Experimental conditions: [Glucose]–0.1–5000 μM, E_{tot}–8 V, [Luminol]–1.5 mM, pH_{rc}/pH_{sc}–10.5/10.75, [GOD]–5 U μL^{-1}, and t_i–2 min. The error bars represent the standard deviations of five independent measurements from different devices.

on the same one batch sensors (intra-assay), the RSD of five parallel measurements was 2.9%. These results suggest that the reproducibility of the C-BP-ECL method was acceptable.

Selectivity is a very important parameter for evaluating a new ECL sensor, especially a sensor with potential applications in biomedical samples. Fig. S6 shows the interference effects of some coexisting species on the detection of 0.1 mM glucose. In our case, a relative error of less than 5.0% was considered to be tolerable. As shown in Fig. S6, the tolerable concentration ratios of coexistent species were 5000-fold for NaCl, 2500-fold for fructose and sucrose, 200-fold for lactose, 30-fold for $FeCl_3$, 20-fold for dopamine (DA), 15-fold for L-ascorbic acid (AA), 3-fold for uric acid (UA) and 1-fold for $CuSO_4$. These results indicated that there was little interference from commonly coexistent substances. Therefore, the proposed C-BP-ECL sensor had an acceptable selectivity for glucose determination.

The long-term storage stability of the sensors is also a key factor in their application and development. In the presented case, it was investigated for about three weeks by monitoring the ECL responses with intermittent usage by every two days. The as-prepared sensors were sealed and stored at 4 °C in a dry environment when they were not in use, and moreover they were used to monitor their ECL responses at intervals of two days (Fig. S7). It can be observed from Fig. S7 that the C-BP-ECL responses measured using the sensors stored for 10 and 20 days decreased to 95.7% and 87.9% of the initial response, respectively. Here, the initial response meant the ECL intensity obtained using the freshly prepared sensors on the "0" day. These results indicated that the proposed sensors had stable storage stability and might be suitable for long-distance transport and analytical applications in remote regions.

3.6. Real sample detection

To evaluate the reliability and application potential of the method, the proposed C-BP-ECL was employed for the determination of glucose in human serum samples. Meanwhile, the clinical hexokinase-based colorimetric method and the commercial glucometer were applied to measure the glucose levels in these samples in parallel. The similarity of the results between the C-BP-ECL and the clinical method (or the glucometer) is shown in Fig. 7. The regression equation of Y = 1.034 × – 0.184 (R^2 = 0.9978) or Y = 0.966 × + 0.549 (R^2 = 0.9957) was achieved correspondingly. It can be seen from the *t*-test estimation in the SI that the glucose concentrations measured by these methods were not statistically different at the 95% confidence level. These results showed that the proposed sensor foreboded great promise as a reliable technique for the determination of glucose in practical applications.

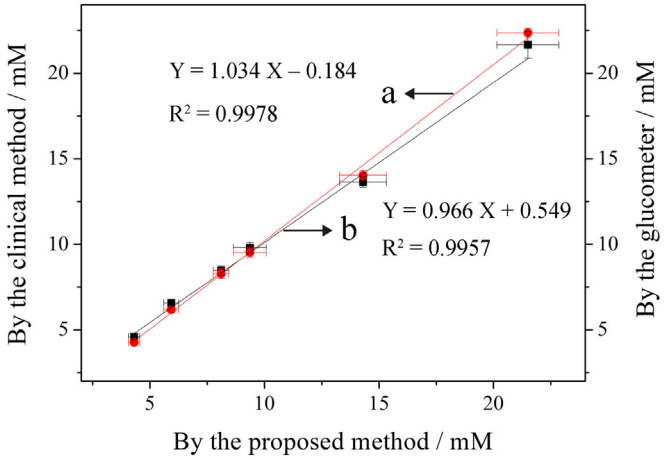

Fig. 7. Comparison of methods for determining glucose concentrations in human serum samples, measured by the clinical method (line a) (or the glucometer, line b) and the proposed method (error bars represent the standard deviations of five measurements from different devices).

4. Conclusions

In summary, we have demonstrated for the first time the coupling of GQDs-AuNPs/PDDA-MWCNTs/CS, C-BP-ECL and cloth-based microfluidics for highly sensitive glucose detection. Through this study, several important findings have been achieved as follows: (1) the fabrication of the sensor with desirable nanostructured electrode surface is simple, rapid, inexpensive and less instrumented; (2) relative to the anodic decoration of C-BPE, the cathodic decoration can produce a stronger ECL signal; (3) based on the desired electrode modification protocol, the proposed sensor has exhibited an about three-orders of magnitude sensitivity enhancement for the detection of glucose; and (4) the glucose concentrations in complex human serum samples can be measured, with high similarity to those determined by two different traditional methods. Therefore, the proposed sensing protocol holds bright prospect for scientific research, biomedical diagnosis, food inspection and so on.

CRediT authorship contribution statement

Dan Wang: Conceptualization, Methodology, Validation, Formal analysis, Investigation, Data curation, Writing - original draft, Visualization. **Yi Liang:** Methodology, Formal analysis, Investigation, Visualization. **Yan Su:** Methodology, Investigation, Visualization. **Qiuping Shang:** Methodology, Investigation. **Chunsun Zhang:** Conceptualization, Methodology, Data curation, Writing - original draft, Writing - review & editing, Visualization, Supervision, Project administration, Funding acquisition.

Acknowledgements

This research is supported by the National Natural Science Foundation of China (81571765), and Guangdong Science and Technology Program (2016A020215143). We thank Dr. Zhiquan queue and Dr. Dayu Liu at Guangzhou First People's Hospital for their help in collecting and assaying the serum samples.

Declaration of interests

None.

Appendix A. Supporting information

Supplementary data associated with this article can be found in the online version at doi:10.1016/j.bios.2019.01.027

References

Amatatongchai, M., Sroysee, W., Chairam, S., Nacapricha, D., 2015. Talanta 133, 134–141.
Arora, A., Eijkel, J.C.T., Morf, W.E., Manz, A., 2001. Anal. Chem. 73, 3282–3288.
Bouffier, L., Arbault, S., Kuhn, A., Sojic, N., 2016. Anal. Bioanal. Chem. 408, 7003–7011.
Budyka, M.F., 2019. Spectrochim. Acta A 207, 1–5.
Chang, B.-Y., Chow, K.-F., Crooks, J.A., Mavré, F., Crooks, R.M., 2012. Analyst 137, 2827–2833.
Chen, X.M., Cai, Z.M., Lin, Z.J., Jia, T.T., Liu, H.Z., Jiang, Y.Q., Chen, X., 2009. Biosens. Bioelectron. 24, 3475–3480.
Clark, L.C., Lyons, C.L.C., 1962. Ann. N.Y. Acad. Sci. 102, 29–45.
Cui, R.J., Huang, H.P., Yin, Z.Z., Gao, D., Zhu, J.J., 2008. Biosens. Bioelectron. 23, 1666–1673.
Dong, Y.Q., Wu, H., Shang, P.X., Zeng, X.T., Chi, Y.W., 2015. Nanoscale 7, 16366–16371.
Feng, Q.M., Chen, H.Y., Xu, J.J., 2015. Sci. China Chem. 58, 810–818.
Feng, Q.M., Pan, J.B., Zhang, H.R., Xu, J.J., Chen, H.Y., 2014. Chem. Commun. 50, 10949–10951.
Fu, E., Downs, C., 2017. Lab Chip 17, 614–628.
Ge, S.G., Zhao, J.G., Wang, S.P., Lan, F.F., Yan, M., Yu, J.H., 2018. Biosens. Bioelectron. 102, 411–417.
Gupta, S., Smith, T., Banaszak, A., Boeckl, J., 2017. Nanomaterials 7, 301.
Haghighi, B., Bozorgzadeh, S., Gorton, L., 2011. Sens. Actuators B 155, 577–583.
Hu, Y.H., Cheng, H.J., Zhao, X.Z., Wu, J.Z.X., Muhammad, F., Lin, S.C., He, J., Zhou, L.Q., Zhang, C.P., Deng, Y., Wang, P., Zhou, Z.Y., Nie, S.M., Wei, H., 2017. ACS Nano 11, 5558–5566.
Jiang, J.J., Chen, D., Du, X.Z., 2017. Sens. Actuators B 251, 256–263.
Karim, Md.N., Anderson, S.R., Singh, S., Ramanathan, R., Bansal, V., 2018. Biosens. Bioelectron. 110, 8–15.
Li, G.X., Lian, J.L., Zheng, X.W., Cao, J., 2010. Biosens. Bioelectron. 26, 643–648.
Li, H.J., Liu, C.L., Wang, D., Zhang, C.S., 2017. Biosens. Bioelectron. 91, 268–275.
Li, X.J., Lu, P., Wu, B., Wang, Y.G., Wang, H., Du, B., Pang, X.H., Wei, Q., 2018. Biosens. Bioelectron. 112, 40–47.
Lin, Z.Y., Chen, J.H., Chen, G.N., 2008. Electrochim. Acta 53, 2396–2401.
Liu, W., Ding, F., Wang, Y.Y., Mao, L., Liang, R.X., Zou, P., Wang, X.X., Zhao, Q.B., Rao, H.B., 2018a. Sens. Actuators B 265, 310–317.
Liu, M., Liu, R., Wang, D., Liu, C.L., Zhang, C.S., 2016. Lab Chip 16, 2860–2870.
Liu, M., Wang, D., Liu, C.L., Liu, R., Li, H.J., Zhang, C.S., 2017. Sens. Actuators B 246, 327–335.
Liu, C.L., Wang, D., Zhang, C.S., 2018b. Sens. Actuators B 270, 341–352.
Liu, X.Q., Niu, W.X., Li, H.J., Han, S., Hu, L.Z., Xu, G.B., 2008. Electrochem. Commun. 10, 1250–1253.
Lou, F.M., Lu, Z.S., Hu, F.X., Li, C.M., 2017. J. Electroanal. Chem. 787, 125–131.
Lu, W.X., Bao, N., Ding, S.N., 2016. RSC Adv. 6, 25388–25392.
Matz, K., Keresztes, K., Tatschl, C., Nowotny, M., Dachenhausenm, A., Brainin, M., Tuomilehto, J., 2006. Diabetes Care 29, 792–797.
Nie, G.M., Wang, Y., Tang, Y., Zhao, D., Guo, Q.F., 2018. Biosens. Bioelectron. 101, 123–128.
Nilghaz, A., Ballerini, D.R., Shen, W., 2013. Biomicrofluidics 7, 051501.
Qiu, B., Lin, Z.Y., Wang, J., Chen, Z.H., Chen, J.H., Chen, G.N., 2009. Talanta 78, 76–80.
Salehnia, F., Hosseini, M., Ganjali, M.R., 2018. Anal. Methods 10, 508–514.
Sang, Y.T., Fu, A.P., Li, H., Zhang, J.T., Li, Z.C., Li, H.L., Zhao, X.S., Guo, P.Z., 2016. Colloid Surf. A 506, 476–484.
Sun, X.L., Wang, H., Jian, Y.N., Lan, F.F., Zhang, L.N., Liu, H.Y., Ge, S.G., Yu, J.H., 2018. Biosens. Bioelectron. 105, 218–225.
Tian, X.T., Lian, S., Zhao, L.M., Chen, X.M., Huang, Z.Y., Chen, X., 2014. J. Solid State Electr. 18, 2375–2382.
Wang, H., Zhou, C.X., Sun, X.L., Jian, Y.N., Kong, Q.K., Cui, K., Ge, S.G., Yu, J.H., 2018. Biosens. Bioelectron. 117, 651–658.
Wang, J., 2008. Chem. Rev. 108, 814–825.
Wang, Y.Z., Xu, C.H., Zhao, W., Guan, Q.Y., Chen, H.Y., Xu, J.J., 2017. Anal. Chem. 89, 8050–8056.
Xiao, Y., Xu, L.R., Qi, L.W., 2017. Talanta 165, 577–583.
Yamada, K., Shibata, H., Suzuki, K., Citterio, D., 2017. Lab Chip 17, 1206–1249.
Yan, J.X., Ge, L., Song, X.R., Yan, M., Ge, S.G., Yu, J.H., 2012. Chem. Eur. J. 18, 4938–4945.
Yao, Y., Zhang, C.S., 2016. Biomed. Microdevices 18, 92.
Ye, C., Zhong, X., Yuan, R., Chai, Y.Q., 2014. Sens. Actuators B 199, 101–107.
Zhao, J.J., Wu, M.S., Tu, Y.F., 2011. Chin. J. Anal. Chem. 39, 985–989.
Zhang, H.J., Li, H.L., Li, X.T., Zhao, B., Yang, J.H., 2014. Int. J. Hydrog. Energy 39, 16964–16975.
Zhang, S.B., Shen, Y.M., Shen, G.Y., Wang, S., Shen, G.L., Yu, R.Q., 2016a. Anal. Biochem. 494, 10–15.
Zhang, X., Ding, S.N., 2017. Biosens. Bioelectron. 94, 47–55.
Zhang, X.W., Zhai, Q.F., Xing, H.H., Li, J., Wang, E.K., 2017. ACS Sens. 2, 320–326.
Zhang, X.W., Zhai, Q.F., Xu, L., Li, J., Wang, E.K., 2016b. J. Electroanal. Chem. 781, 15–19.
Zhong, X., Chai, Y.Q., Yuan, R., 2014. Talanta 128, 9–14.
Zhou, Z.Y., Xu, L.R., Wu, S.Z., Su, B., 2014. Analyst 139, 4934–4939.
Zhu, L.D., Li, Y.X., Zhu, G.Y., 2002. Sens. Actuators B 86, 209–214.